PCCP

Accepted Manuscript

ROYAL SOCIETY OF CHEMISTRY

www.rsc.org/pccp

Stochastic Atomistic Simulation of Polycyclic Aromatic Hydrocarbon Growth in Combustion

Jason Y.W. Lai, Paolo Elvati, Angela Violi*

Department of Mechanical Engineering, University of Michigan, Ann Arbor, MI 48109-2125, USA

Abstract

Nanoparticles formed in gas phase environments, such as combustion, have important impact on society both as engineering components and hazardous pollutants. A new software, the Stochastic Nanoparticle Simulator (SNAPS) was developed, applying a stochastic chemical kinetics methodology, to computationally investigate the growth of nanoparticle precursors through trajectories of chemical reactions. SNAPS was applied to characterize the growth of polycyclic aromatic hydrocarbons (PAHs), important precursors of carbonaceous nanoparticles and soot, in a premixed laminar benzene flame, using a concurrently developed PAH growth chemical reaction mechanism, as well as an existing benzene oxidation mechanism. Simulations of PAH ensembles successfully predicted existing experimentally measured data and provided novel insight into chemical composition and reaction pathways. The most commonly observed PAH isomers in simulations showed the importance

*Corresponding author.
Tel: +1(734)615-6448; Fax +1(734)647-9379
E-mail Address: avioli@umich.edu
Postal Address: 2250 G.G. Brown Laboratory, 2350 Hayward Street, Ann Arbor, MI, 48109-2125, USA

of 5-membered rings, which contrasts with traditionally assumed compositions involving primarily pericondensed 6-membered rings. In addition, the chemical growth of PAHs involved complex sequences of highly reversible reactions, rather than relatively direct routes of additions and ring closures. Furthermore, the most common reactions involved 5-membered rings, suggesting their importance to PAH growth. The framework developed in this work will facilitate future investigation of particle inception and soot formation and will benefit engineering of novel combustion technologies to mitigate harmful emissions.

1. Introduction

Nanoparticles (size $\leq$ 100 nm) formed in gas phase environments are prevalent in modern society as components in engineering and effluents from industrial processes [1]. For example, flame synthesis accounts for the majority of commercial nanoparticles, with typical production rates on the order of at least 100 metric tons per day [2]. The difficulty in studying these processes experimentally motivates the development of computational tools for exploring and characterizing the growth of nanoparticles and their precursors. The current work discusses the development and application of a new software for stochastic simulation of chemical growth of nanoparticle precursors, named the Stochastic Nanoparticle Simulator (SNAPS). Broadly, this software applies kinetic Monte Carlo to simulate chemical reaction trajectories for individual molecules, in order to enable the investigation of the chemical and physical properties of particles distributions that are produced from different sequences of elementary reactions. SNAPS is based on the philosophy of the

previously developed Atomistic Model for Particle Inception (AMPI) model [3, 4], which aims to describe carbonaceous particle growth and morphology via elementary chemical reactions.

The current SNAPS methodology has been implemented in an entirely new Python code base and contains many practical and methodological enhancements, representing a substantial new development. Key new features include improved computational performance, as well as novel schemes for defining chemical reactivity and reaction rejection, the latter of which accounts for steric hindrance as well as imperfections in defined chemical growth mechanisms. Currently, the development of SNAPS has focused on the context of carbonaceous nanoparticle (CNP) precursor growth in combustion, namely simulation of ensembles of polycyclic aromatic hydrocarbons (PAHs). However, SNAPS was developed to be extensible, with the future aim of simulating growth beyond single molecules, including particle aggregation and nucleation, as well as other nanoparticle growth systems. Such processes include the formation of titania, silica, or the nanoscale transition (t)-aluminas, which are formed through flame processes [5, 6].

CNPs are an important class of nanoparticles, having both useful applications as well as harmful health effects. For example, carbon black is the most important commercial nanoparticle [2], and CNPs can function as a cathode catalyst in solar cells [7]. Conversely, CNPs also pose significant danger as pollutants emitted from internal combustion engines, both as nanoparticles and as larger carbonaceous aggregates known as soot. The primary components of CNPs are PAHs, which are classified as carcinogenic by the International Agency for Research on Cancer [8]. Moreover, the small size of CNPs

may increase their toxicity [9] and there have been efforts [10–13] to understand the transport of CNPs in biological systems as a way to assess toxicity. These studies utilize a computational framework to investigate the interactions of CNPs cellular membranes. Since morphology greatly influences these interactions and toxicity [14, 15], there is strong motivation to understand the formation and composition of CNPs. This knowledge is important for designing strategies for emission control and mitigating negative health effects. A key knowledge gap in CNP formation is particle inception, or nucleation, which delineates the transition from the gas to solid phase. Inception is a complex process involving both chemical and physical phenomena [16] and has a significant impact on the growth of combustion emitted particles, especially their size distribution [17] and morphology. There is a substantial body of work, reviewed previously [5, 16, 18–24], that has investigated carbonaceous nanoparticles and soot formation in combustion. Although nucleation is expected to involve PAHs, the exact mechanisms involved remain poorly understood. This array of work illustrates the considerable uncertainty in the chemical composition and morphology of nascent PAHs, which heavily impact particle inception. Therefore, characterizing the formation, chemical composition, and morphology of PAHs is a key step in understanding CNP and soot formation.

In this work, SNAPS has been applied to study the chemical growth of PAHs. This application contrasts with traditional studies using continuous deterministic models, which describe the time evolution of species concentrations using coupled ordinary differential equations and are valid and efficient when describing a system in the thermodynamic limit [25]. As a result of

this efficiency, chemical kinetic mechanisms [26–33] and combustion models, such as those in CHEMKIN [34], have widely been used to study combustion and PAH growth. A more general approach, employed by SNAPS, is to use a discrete stochastic formulation of chemical kinetics to describe the reactivity of individual molecules, producing detailed sequential reaction trajectories. This formulation of chemical kinetics is consistent with the physical nature of chemically reacting systems as discrete molecules that move and react randomly [25]. Importantly, large ensembles of these trajectories represent macroscopic information about the system, equivalent to the deterministic formulation. Despite increased computational expense, a stochastic approach offers the benefit of chemical detail at both the molecular and macroscopic scale.

SNAPS was developed concurrently with a PAH growth mechanism and was utilized to simulate and characterize the formation of PAHs in a premixed laminar benzene flame [35]. These simulations performed well in predicting experimentally measured species concentration ratios and mass distributions of PAHs. Ensembles of PAH growth trajectories were then analyzed to investigate the rate of mass accumulation by chemical growth; the most frequently observed PAH structures associated with mass distribution peaks; and the most important chemical reaction pathways. The results of this analysis highlighted that PAH growth by chemistry is substantially more complex than the linear addition of acetylenes forming pericondensed aromatics with primarily 6-membered rings. Specifically, 5-membered rings are prevalent among sampled PAH species and their growth involves complex sequences of highly reversible reactions. Consequently, the variety of potential PAHs

increases dramatically with size. Since chemical composition and morphology influences physical aggregation, characterizing the structures of nascent PAHs will greatly advance understanding of particle inception. The results of this work provide new insight into the detailed structure of PAHs and will inform the further development of models for particle inception and soot growth.

2. Methodology

2.1. SNAPS: The Stochastic Nanoparticle Simulator

The Stochastic Nanoparticle Simulator (SNAPS) is a stochastic model for simulating chemical growth of particles. Given a set of chemical reactions, environmental conditions, and an initial "seed" molecule, SNAPS simulates the trajectory of sequential reactions of a single particle, depicted in Figure 1. A typical SNAPS trajectory will represent one of many possibilities, due to the probabilistic nature of the method. General insight into the growth process requires the analysis of a large ensemble of trajectories.

SNAPS has a new code base, leveraging Python and libraries for scientific computing including cheminformatics functionality [36]. Additionally, relative to AMPI, the software includes a new scheme for defining chemical reactivity and the compartmentalization of growth chemistry as an component or input to the code; a new potential energy scheme to account for steric factors and imperfect reaction definition; and greatly increased computational speed. These developments address scientific and practical issues and also greatly expand the extensibility of the code, towards the secondary goal of expanding the software to simulate additional growth phenomena.

The foundation of SNAPS remains kinetic Monte Carlo, due to its computational efficiency in modeling the long time scale of CNP growth. Kinetic Monte Carlo, described in detail elsewhere [37–40], is a stochastic method for modeling a rare-event system. In the current context, the chemical reactions of a growing molecule can be considered rare events, which occur infrequently and on a fast time scales relative to the time spent "wandering" in the gas phase between collisions and/or reactions, such that the molecule maintains no memory of previous reactions. SNAPS employs an iterative algorithm to compute each successive reaction step, which broadly proceeds as follows:

1. **Search**: Builds a weighted list of possible chemical reactions, based on the structure of the molecule, a given reaction mechanism, and the gas phase environment.
2. **Selection**: Selects a reaction using the Bortz, Kalos, and Lebowitz (BKL) algorithm [38]. Tests this choice based on the change in energy, ΔE, of reaction. If the reaction is rejected, this step is repeated, omitting the rejected reaction.
3. **Execution**: Applies appropriate modifications to the molecular structure, advances the time of simulation according to the BKL algorithm, and checks for termination of simulation based on a specified stop criterion, e.g. time of simulation, size of molecule, or number of kMC steps.

Each reaction in the list of possibilities is weighted by its corresponding kinetic rate, k_{ij}, which is computed using phenomenological rate laws for first and second order reactions. Each rate depends on an input rate constant, as well as the concentration of any associated gas phase species in the case of a

bimolecular reaction. A reaction is then selected using the BKL or "direct" algorithm. Summation of each of reaction rate sequentially creates an array, s, of partial sums, where element $s(j)$ represents the sum of all reactions up to and including reaction j,

$$s(j) = \sum_{q}^{j} k_{iq}$$

Figure 2 depicts the BKL algorithm. The array s is analogous to a one dimensional object of length k_{tot} that is divided into sections. Each section corresponds to a specific reaction and has a length equal to k_{ij}. Selection of a reaction amounts to randomly choosing a point along this object and retrieving the reaction corresponding to the section containing this point. Algorithmically, a random number r_1 is drawn from a uniform distribution in the range (0,1) and multiplied by k_{tot}. The first element in the array s for which $s(j) > r_1 k_{tot}$ represents the selected pathway. The time of the simulation is advanced according to

$$\delta t_{kMC} = \frac{-\ln(r_2)}{k_{tot}}$$

$$k_{tot} = \sum_{j} k_{ij}$$

where r_2 is a second randomly chosen number from a uniform distribution in the range (0,1).

Strictly speaking, SNAPS simulates the growth of a seed molecule or particle in well mixed, dilute, and ideal gas phase systems. Inputs that describe the environment for growth must be provided as inputs to the algorithm. These inputs include temperature, pressure, and ambient gas phase species,

such as hydrogen radicals, hydroxyl radicals, or acetylene. While direct simulation of combustion is not within the scope of SNAPS, the program can simulate representative growth of particles in such environments given appropriate profiles. For example, an SNAPS simulation can represent the growth of a single particle in a zero-dimensional homogeneous combustion reactor, or one as it travels along a streamline in a flame.

Conventional kinetic mechanisms, such as those used with the CHEMKIN software, specify all reactants, products, and intermediate species, as well as the chemical reactions that form and consume each one. Such a model is consistent with the macroscopic formulation of a deterministic simulation. However, since SNAPS employs a stochastic formulation of chemical kinetics, it requires a significantly different description of chemical reactivity in the specification of a growth model. Namely, SNAPS describes chemical reactivity from the perspective of the single growing molecule, rather than the reacting system as a whole. Consequently, the chemical growth model must be defined in SNAPS such that it describes the reactivity of the growing molecule at any step in its trajectory. This requirement necessitates flexibility and consistency in the specified growth model.

SNAPS defines chemical reactivity using a new scheme using the Smiles Arbitrary Target Specification (SMARTS) [41] language for specifying substructure patterns within a molecule. Using SMARTS, reaction sites are specified in terms of properties including atom type (e.g. aromatic, aliphatic, sp^3 hybridized), bond type, and molecular connectivity (e.g. membership in ring(s) or specific aliphatic group). This functionality enables great precision and flexibility in reaction definition. Then, reactions are defined in terms of

these reaction sites and corresponding kinetic rate constants.

SNAPS also employs a new scheme for reaction rejection to address growth model limitations, namely steric factors and imperfect reaction definitions. Steric hindrance occurs when the algorithm attempts an addition reaction at a position of the particle where there is insufficient physical space to accommodate the incoming species. Additionally, there are instances where the algorithm erroneously identifies unphysical chemical reactions, such as for ring closures, that have identical connectivity to a legitimate chemical reaction. In theory, the kinetic rates for these incorrect reactions should be vanishingly low and they should not be available for selection; inclusion of these reactions is an unfortunate result of the simplifications made in the chemical growth mechanism, which assigns them the same rate as a legitimate reaction. Figure 3 depicts examples of steric hindrance and an unphysical reactions that SNAPS will reject, including incorrect additions of benzene and ring closures.

The SNAPS algorithm implements a scheme that exploits the large increases in the potential energy that accompany these unphysical reactions. In each kMC step, SNAPS employs an energy minimization step that computes the change in potential energy, $\Delta E_{reaction}$, between initial and final states of the system due to the chosen reaction. The change in potential energy is then related to a probability of reaction, $P(\Delta E_{reaction}) = \exp(\beta \Delta E_{reaction})$, where $\beta = \frac{1}{k_B T}$ and k_B is Boltzmann's constant. $P(\Delta E_{reaction})$ is the ratio of the Boltzmann factors for the initial and final states of the chosen reaction, including all associated reactants and products. Consequently, the probability of reaction decreases exponentially with an increase in positive reaction

energy. If this probability falls below a user defined threshold, the reaction is rejected. This scheme was chosen because it enables the specification of a threshold that accounts for the temperature of the system.

As an example, for reaction energy of 100 $\frac{kcal}{mol}$ at 1500K, a typical combustion temperature, $P(\Delta E_{reaction}) = 2.6^{-15}$. Conversely, for a reaction energy of 10 $\frac{kcal}{mol}$ at 1500K $P(\Delta E_{reaction}) = 0.035$. The example reaction probabilities show a large decrease with an increase of a single order of magnitude in energy, which facilitates the choice of rejection threshold. Currently, the reaction rejection threshold has been chosen in order to exclude unphysical reactions, such as those shown in Figure 3, which result in extreme increases in system energy. These reaction energies are several orders of magnitude greater than those for physical reactions. Therefore, in the current work, we reject reactions for which $P(\Delta E_{reaction}) < 10^{-7}$, which is sufficient to filter out unphysical reactions.

2.2. Simulating PAH Chemical Growth

A new growth model for SNAPS has been developed to investigate PAH formation in combustion. An important goal in developing this model was to implement major PAH chemical growth pathways. These reaction pathways were translated to SNAPS in terms of their elementary steps, in order describe the reactivity of any given intermediate species. Then, utilizing the stochastic nature of individual trajectories, SNAPS simulations were used to explore the PAHs predicted by the combination or mixing of reaction pathways. Therefore, the pathways in the current description are meant to be examples of growth, rather than an exhaustive list.

The base collection of pathways for the current PAH growth model is the

hydrogen abstraction, acetylene addition (HACA) mechanism [16, 31]. This mechanism is important in PAH growth because it involves acetylene and hydrogen radicals, which are among the most abundant species in flames [5]. As a result, HACA is considered to be the most important PAH chemical growth mechanism and is the foundation of many PAH kinetic models. As the name implies, HACA is a repetitive sequence of hydrogen abstractions and acetylene additions that result in an increasing number of aromatic rings. The current implementation of this mechanism for SNAPS combines several variants of the HACA mechanism [26, 31, 42–44], utilizing chemical rate constants derived from Kislov et al. [45].

The growth model also includes addition reactions ethylene and vinyl radicals, which are 2 carbon species that may also contribute to growth via the HACA mechanism. Furthermore, the mechanism includes the addition of benzene, phenyl, and propargyl radicals, which can form biphenyl moieties; cyclopentadienyl radicals, forming phenanthrene moieties; and methyl radicals, which can, for example, contribute to the formation of indene moieties. Many different types of ring closures were also included in the mechanism, including creation of 5- and 6-membered rings at "zig zag," "armchair," and "bay" sites (nomenclature described by Celnik et al. [46]), using rates derived from Kislov et al. [45], Raj et al. [47], and Violi [48]. The included pathways have been proposed in literature as significant contributors to PAH growth and have been included in previously developed chemical kinetic mechanisms [26, 30, 49, 50]. A full description of the PAH growth model, including reaction pathway diagrams and tables that enumerate the chemical reactions and rate constants has been provided as supplementary information.

Reaction rates have been sourced from a variety of existing literature, with preference for rates computed using *ab initio* methods and reaction rate theory. Unimolecular rates in the current model have been used in the high pressure limit. While efforts were made to source accurate data, analogous chemical rates were used to estimate those for reactions where specific data was not available. In particular, many rates for reverse reactions have not been explicitly computed or reported. Each missing reverse reaction rate was estimated by using the relationship between forward and reverse rate constants at equilibrium, using equilibrium constants computed using existing NASA polynomial thermodynamic data. While there is error associated with this type of estimation, this method aligns the calculated rates with existing deterministic chemical mechanisms which estimate reverse rates in the same way. As a result, these computed reaction rates will have equivalent accuracy to implicitly computed reverse reaction rates in a traditional deterministic chemical kinetics simulation, such as in CHEMKIN.

There is an emphasis on reaction reversibility in the current work that arises from the desire to observe PAH growth as accurately as possible. Fundamentally, reversibility is a requirement of the kinetic Monte Carlo (kMC) methodology when modeling a chemical system like PAH growth. Beyond this theoretical requirement, intuitively, a given PAH does not necessarily grow in a linear sequence of, for example, hydrogen abstraction and acetylene addition. Indeed, reversibility is a fundamental and important characteristic of the HACA mechanism [16]. Therefore, the inclusion of reverse reactions is paramount to describing the complex sequence of chemical reactions that comprise the growth trajectory of a given PAH and produces

a more physically realistic growth trajectory. Reversibility enables the description of intramolecular structural rearrangements, enhances the mixing of the elementary steps in the growth model, and therefore greatly expands the accessible space of PAH structures that can be explored using SNAPS.

A drawback of emphasizing reaction reversibility is a common issue in kMC applications where some reactions have significantly lower barriers than competing reactions. These low barrier reactions are the most likely to be chosen by the kMC algorithm, leading to inefficiency in sampling states separated by higher barriers. Consequently in SNAPS, the specified growth model greatly impacts computational performance. Corresponding forward and reverse reactions with large rates in the growth model, due to low barriers or faster kinetics, lead to trajectories where particles spend substantial time switching between the same two structures. For example, a particle may experience repeated cycles of hydrogen abstraction followed by hydrogen addition. While this behaviour is physically correct, it results in computational inefficiency, especially in growing particles of large size. Currently, this type of issue is mitigated by the significant speed improvement of SNAPS, which enables the simulation of these reversible reactions while maintaining practical overall run times. The simulation results discussed later demonstrate the reversibility of reactions, as well as the increase in computational speed. Further amelioration of this problem could involve modifying the reaction model to define global reactions that jump over these elementary steps and obviate simulation of these repetitive cycles. However, this approach greatly hinders the exploration of PAH structures that may result from this reversibility and has been avoided as much as possible.

Since SNAPS uses the growth model to specify potential reactions for any intermediate species, it typically necessitates the definition of lumped reaction types. For example, instead of defining separate rates for hydrogen abstraction from benzene and naphthalene, these chemical reactions are lumped and defined as hydrogen abstraction from an aromatic carbon-hydrogen pair. Lumping such reactions requires the choice of a single rate to approximate all reactions in the set. For hydrogen abstraction by H, Kislov et al. [45] computed different chemical rates for benzene and naphthalene. The current SNAPS model approximates the rates of hydrogen abstraction from an aromatic carbon as the rate for benzene. Moreover, to derive a single rate for the corresponding SNAPS hydrogen abstraction reactions, these rates must be adjusted for reaction path degeneracy. Similarly, other reactions, such as ring closures or acetylene addition, have been simplified. The simplification of the HACA mechanism in this manner is a design choice, considering the detail of mechanism definition with accuracy of the simulation and computational performance. A complete description of PAH growth will require an impractically detailed mechanism and thus necessitated the simplification of lumping reactions. These reaction rates and types are given in the description of the growth model given as supplementary information.

2.3. PAH Growth in a Premixed Laminar Benzene Flame

SNAPS and the new PAH growth model were applied to study the formation of PAHs in a premixed laminar benzene flame, originally studied by Tregrossi et al. [35]. This flame was first simulated using CHEMKIN [34] and the benzene oxidation and PAH mechanism of Richter et al. [50] to compute spatially dependent temperature and gas phase species profiles. Among sev-

eral other mechanisms [26, 30, 51] compared in simulations of this flame, this mechanism best predicted the concentration profile of acetylene, which is a key species in PAH growth due to its high concentration. Predictions of other species profiles, such as benzene, carbon dioxide, ethylene, cyclopentadiene, naphthylene, and acenaphthylene were similar among compared mechanisms. These spatial profiles were converted to temporally dependent ones, assuming a PAH traveling downstream along the center streamline with computed axial velocities within each spatial grid interval. These temporal profiles served as inputs to SNAPS simulations of PAH ensembles.

Furthermore, SNAPS simulations were started at a height of 4.5 mm above the burner, which corresponds to a point just before the peak concentration of H radicals and acetylene concentration. This point approximately locates the maximum rate of production of H radicals and acetylene, suggesting that they are consumed significantly after this point. Simulations started at this point in the flame traverse the main reaction zone of the flame and this location therefore can be considered to be the main starting point for PAH growth. Simulations were stopped at a simulation time corresponding to the end of the laminar flame environment, or the end of the computed temporal temperature and gas phase species profiles. The seed molecule for simulations was chosen to be benzene. Since SNAPS currently does not directly simulate the combustion environment, the implicit assumption of the current trajectories is that the distribution of PAHs downstream primarily consist of those that began as benzene at this point in the flame. This assumption was also tested through comparison with experimental data.

SNAPS simulations were also analyzed to classify the most important

PAH structures for specific mass ranges. To simplify analysis of the vast amount of potential structures, PAHs were classified by carbon configuration using social permutation invariant (SPRINT) topological coordinates [52], which utilize graph theory to describe the connectivity of an isomer. SPRINT coordinates were computed for each SNAPS trajectory. Importantly, PAHs with equivalent connectivity will have almost identical SPRINT coordinates, which are invariant under all permutations of a set of N atoms. Isomers with specific carbon numbers were grouped, focusing specifically on carbon-carbon connectivity, by placing a limit on the p-2 norm of the difference between the vectors representing the SPRINT coordinates of each pair of PAHs in the target ensemble. This p-2 norm threshold was adjusted to produce distinct carbon configurations for the top 5 most frequently observed PAH structures.

3. Results and Discussion

3.1. Comparison with Experimentally Measured Quantities

In order to verify the performance of the SNAPS algorithm and the PAH reaction mechanism, simulations of PAH growth were analyzed and compared with experimentally measured data [35]. An ensemble of 30000 SNAPS trajectories was used to compute a distribution of species, which was compared with ratios of experimentally measured concentrations in the flame of Tregrossi et al. [35], including naphthalene, acenaphthylene, biphenyl, indene, phenanthrene, and anthracene. These ratios were computed in order to be able to compared results among the CHEMKIN, experimental, and SNAPS results. In addition, the chosen set of ratios include species that are formed through different reactions. For example, the formation of indene can occur

through the addition of methyl and acetylene radicals; biphenyl can be produced through the addition of a phenyl radical or benzene; and acenaphthylene, naphthalene, phenanthrene, and anthracene can be produced through HACA mechanism. This set of comparisons demonstrates the functionality of SNAPS and the PAH mechanism. The same trajectories were also used to compute PAH mass distributions at heights of 8 and 10 mm above the burner, which correspond to simulation times of 15 and 23 ms, respectively. Figure 4 compares experimentally measured concentration ratios with those computed using CHEMKIN and SNAPS. Additionally, Figure 5 shows a comparison of computed and experimentally measured mass distributions, with the experimental values restricted to peaks for clarity.

In the comparison of species concentration ratios shown in Figure 4, the time evolution of the SNAPS species ratios at the short simulation times (before approximately 5 ms) show a correlation with the chosen starting point, resulting in significant deviation from both CHEMKIN and experimental profiles. Nevertheless, the simulations are able to achieve reasonable accuracy after approximately 5 ms, which correspond to the regions of primary interest. Importantly, the SNAPS results are limited in accuracy by their environmental inputs, which in this case come from CHEMKIN solutions. Compared with CHEMKIN, SNAPS predictions are very similar in performance to the deterministic solutions. Additionally, SNAPS simulations well predict the experimental mass distributions measured at both heights above the burner. The accuracy of these predictions provides strong verification of the SNAPS algorithm as well as the PAH growth model. The SNAPS model captures correct distributions of both PAH mass and gas phase species, ex-

plores a vast variety of growth trajectories, and provides detailed molecular structures. The exploratory nature of this stochastic perspective is its primary strength, facilitating the evaluation of proposed reaction rates and pathways, as well as discovery of the most important PAH structures. In this case, the developed PAH mechanism, especially HACA, well predicts growth and corroborates the importance of these reaction pathways.

3.2. Computational Performance

The computational speed of SNAPS was compared with AMPI in order to demonstrate its substantial performance improvement. SNAPS is a substantially faster software than AMPI, but a direct comparison of absolute speed is difficult, due to the difference in chemical growth mechanisms implemented in each software. Nevertheless, performance per kMC cycle was evaluated against AMPI simulations for 100 trajectories of chemical growth up to 30 atoms. The average times per kMC cycle for AMPI and SNAPS were 48.56 and 0.4273 seconds per cycle, respectively. The average kMC cycle time illustrates the efficiency of the SNAPS algorithm. SNAPS outperformed AMPI by approximately 113 times on a per cycle basis.

3.3. Mass Accumulation

An important aspect of particle inception and soot formation is the rate of mass growth. The role of the current chemical reaction pathways in PAH mass growth was investigated by comparing the time evolution of average mass growth predicted by SNAPS simulations in two different environments related to the current benzene flame. The first environment was time dependent corresponding to the benzene flame. The second environment was

constant, corresponding to the flame conditions at a height of 5.2 mm above the burner. The latter conditions were chosen to represent the ideal environment for chemical growth in this flame. Figure 6 compares the average mass over time for both simulations. While PAHs in the ideal environment grow steadily, those growing in the real flame environment reach a plateau. This stagnation in growth corresponds to the depletion of H radicals and decrease in temperature outside of the main chemical reaction zone of the flame. These high radical concentrations are therefore very important to the chemical growth of PAHs, which can be ascribed to the importance of hydrogen abstraction reactions in the HACA mechanism. Therefore, although these chemical reactions, in ideal conditions, lead to continuous particle growth, they have a limited role under the current flame conditions, specifically in regions of high radical concentration and temperature.

Since experiments have observed particles much larger than the approximate 200 amu plateau shown in Figure 6, a reasonable conclusion from these simulations is that additional mechanisms must be involved in particle inception and growth, including, for example, hitherto neglected chemical reactions or faster kinetic rates. Another potential mechanism is growth via physical agglomeration of PAHs. Previous work [5, 16, 31] has argued that particle inception by purely chemical reactions is insufficient to predict observed nucleation rates, suggesting physical agglomeration as a complementary process. In addition, comparison with experimentally measured bimodal particle size distributions [5, 53] shows that nucleation models using physical agglomeration correctly predict this bimodality, while those using purely chemical growth erroneously predict a unimodal distribution. These

SNAPS simulations therefore show that additional work must investigate and quantify more growth pathways to deepen our understanding of particle inception.

3.4. PAH Structures and Reaction Pathways

Understanding the composition and morphology of PAHs formed in combustion is a key step in understanding particle inception and soot formation. This task is an ideal application of SNAPS, which explores detailed molecular structures. Accordingly, the distribution of PAH structures was investigated for the mass frequency peaks between 200 and 400 amu. Figure 7 shows the top 5 most frequently observed carbon structures in 5000 trajectories for carbon counts between C16 and C32 at a height of 8 mm above the burner (simulation time of 15 ms), which correspond to masses around 202 and 400 amu, respectively. There is a range of PAH masses around each peak that correspond to species with the same number of carbons, but a different number of hydrogen atoms. Since the carbon skeleton of these PAHs are of the most interest, hydrogens were neglected and these species were analyzed as a group. The most important feature of these structures is the prevalence of 5-membered rings, which contrasts with conventional assumptions about the composition of PAHs. Prominent PAH masses have traditionally been associated with almost exclusively 6-membered ring PAHs, such as pyrene, or coronene. These types of species are commonly referred to as "Stein's Stabilomers" and are considered to be prevalent based on their high thermodynamic stability, as argued by Stein and Fahr [54].

In the current results, several observed structures do correspond with proposed stabilomers, but these species contain 5-membered rings. For example,

the structure for C16 column A in Figure 7 and pyrene (C16 column D), were identified as a stabilomer by Stein and Fahr. Interestingly, the former structure was observed with 74.9% frequency, while pyrene was observed far less often, with a frequency of 0.948%. Likewise, C18 column C, C22 column A, and C24 column A correspond to proposed stabilomer species that do not contain exclusively 6-membered rings. These results suggest the importance of 5-membered rings in PAH growth and also support the exploration of additional reaction mechanisms for 5-membered rings, including their conversion to 6-membered rings, to better simulate PAH growth. Figure 7 also shows a wide variety of structures that are not contained in the traditional PAH stabilomer grid. This phenomenon is particularly notable for a carbon count of 32, where the most commonly observed structure occurred with a frequency of only 17.4%, the top 5 most frequent structures accounted for only 39.4% all those observed, and the total number of distinct structures classified was 166. Physically, this variety of structures arises from a substantial increase in potential reactions and branching pathways with molecule size. The five structures shown in Figure 7 illustrate the variety in possible PAH features, including both planar molecules, attached chains, and configuration of of 5- and 6-membered rings. Additionally, curved species, were a 5-membered ring is enclosed by five 6-membered rings, were also observed in smaller quantities.

The variety of structures in Figure 7 arise from complex sequences of reactions, which were recorded throughout SNAPS simulations. Simulation trajectories were analyzed to determine the relative frequencies of each reaction. Figure 8 illustrates some of the most common reaction pathways observed throughout simulations. Each forward and reverse reaction is annotated with

its frequency relative to all recorded reactions. The most common reactions were the forward and reverse hydrogenation of 5-membered rings, the first step of the ring opening pathway shown in Figure 8a, with a frequency of 26.8% and 24.8% respectively. The uncertainty in all rates included in the PAH mechanism leads to the question of whether the importance of this hydrogenation reaction is correct. The rate for hydrogenation was taken from the work of Frenklach et al. [55] who assigned it based on analogy with the reaction $C_2H_4 + H \rightleftharpoons C_2H_5$ in the GRI mechanism [56]. This rate is much higher than those assigned for hydrogen abstraction and thus tends to dominate whenever 5-membered rings are present. The simulation is accurate within the input reaction rates and therefore, part of this analysis is the evaluation of these reaction pathway and rates.

An argument could be made that the dominance of 5-membered ring opening and migration hinders PAH growth by preventing particles from following other reaction pathways, such as growth through the HACA pathway. To test this argument, simulations were run without the 5-membered ring migration pathway in Figure 8a. These simulations were unable to reproduce the previous successful predictions of experimental mass distributions shown in Figure 5. Instead, the predicted mass distributions showed reduced PAH growth, namely substantial decreases in higher masses and increases of lower masses, especially those with 16 carbons. This increase can be ascribed to the high frequency of the structure C16 column A in Figure 7, which contains two 5-membered rings. Without 5-membered ring migration, the particle has fewer reaction pathways to follow, leading to the observed stagnation in growth. Consequently, these results highlight the importance

of reaction pathways involving 5-membered rings, regardless of the absolute accuracy of the specific migration pathway investigated. Future work should aim to deepen understanding of all PAH chemical pathways, especially those involving 5-membered rings.

In addition, reversibility was prominent throughout simulations, as corresponding forward and reverse reactions occured with almost equal frequencies. For example, as shown in Figure 8b, acetylene addition had a frequency of 6.43%, while its reverse reaction had a frequency of 5.99%. As well, ring closures were similarly reversible, exhibited in the last step of Figure 8b, where the forward and reverse reactions forming napthyl had frequencies of 3.12% and 3.00%, respectively. This reversibility illustrates the high degree of reaction pathway mixing and intramolecular rearrangement. For example, in Figure 7 there is no obvious direct route, such as an acetylene addition and ring closure, between the species in C18 column B and those in C20 columns A and B. Instead, the simulations suggest that much of the growth from C18 to C20 requires a more complex sequence of forward and reverse reaction steps, including such as ring closure/opening and acetylene addition/removal.

Out of all the addition reactions in the current mechanism, acetylene accounted for the majority, 98%, of all addition reactions. This dominance can be ascribed to the far greater concentration of acetylene in the flame, typically at least 2 orders of magnitude greater than species such as propargyl or vinyl radicals. Benzene and phenyl were expected to make an important contribution to PAH growth based on their expected abundance as fuel components, but CHEMKIN simulations show that their concentrations fall below

acetylene in the regions of major PAH chemical growth. This phenomenon corroborates the importance of the HACA pathway in PAH chemical growth.

These simulations also demonstrate the importance of kinetics in PAH growth. Previously, in an investigation of a low pressure benzene flame, Weilmünster et al. [57] proposed PAH growth pathways involving both 6-membered and 5-membered rings. These pathways are analogous to those shown in Figures 8c (5-membered ring closure at a zig zag site) and 8b (6-membered ring closure). Weilmünster et al. argued that the 6-membered ring growth pathway is more prominent based on the relatively lower activation energies of its constituent reactions compared with the 5-membered ring growth pathway. However, the formation of a 6-membered ring typically involves the addition of 2 acetylenes, as in Figure 8b. Conversely, only a single acetylene addition reaction is required to create a potential 5-membered ring zig zag closure site, as in Figure 8c. Once this acetylene is added, SNAPS simulations show that the particle is far more likely to experience the unimolecular ring closure step before it reacts with an additional acetylene that would enable a 6-membered ring closure. Therefore, while the closure of a 6-membered ring may have a lower activation energy than a 5-membered ring, due to lower ring strain, the closure of 5-membered rings tends to be more kinetically favourable. Corroborating this conclusion, Weilmünster et al. previously observed that, for a given reaction pathway branch between 5- and 6-membered ring species, the maximum concentration associated with the 5-membered branch was double that of the 6-membered one [57].

4. Conclusions

The newly developed software SNAPS is a stochastic model for chemical growth and contains significant enhancements over its predecessors, including improved schemes for chemical reactivity and reaction rejection, as well as new and extensible code base for future expansion. Along with a concurrently developed PAH chemical growth model, SNAPS successfully predicted experimentally measured species concentration ratios and mass distributions in a premixed laminar benzene flame [35]. These simulations were analyzed to further characterize PAH growth in this flame. The time evolution of average particle mass showed that PAHs do not grow infinitely via chemical reactions, instead only experiencing significant growth in the region of the flame with high radical concentrations and temperature. Furthermore, social permutation invariant (SPRINT) topological coordinates were used to group PAH isomers associated with mass distribution peaks by carbon-carbon connectivity. These isomers exhibited significant presence of 5-membered rings, which correspond to species on the stabilomer grid of Stein and Fahr [54]. Importantly, these PAHs are different from those commonly associated with important PAH masses, such as pyrene or coronene, which have exclusively 6-membered rings. The prevalence of 5-membered rings can be ascribed to the faster kinetics of 5-membered ring pathways that require only a single acetylene addition, compared with 6-membered ring pathways that require two. Analysis of reaction pathways showed the importance of acetylene addition, reversible reactions, and molecular rearrangement, which was also reflected in observed PAH structures that are not connected via a direct growth pathway. These results demonstrate the utility of atomistic simulation in elucidating

features of PAH growth typically inaccessible to experiment, as well as the complexity of PAH growth beyond traditionally held assumptions. SNAPS is also useful in evaluating proposed chemical reaction pathways. This worked showed that the 5-membered migration pathway of Frenklach et al. [55] was necessary to properly predict experimental mass distributions of PAH growing in a premixed laminar benzene flame, and therefore supports continued exploration of PAH growth pathways involving 5-membered rings. The characterization of PAHs in this work will inform future development of models for chemical and physical nanoparticle growth and deepen understanding of particle inception.

Acknowledgements

This work is supported by the US Department of Energy, Division of Chemical Sciences, Geosciences, and Biosciences, Contract No. DE-SC0002619. Jason thanks the Natural Science and Engineering Research Council of Canada for his NSERC PGS-D graduate fellowship.

References

[1] S. K. Friedlander and D. Y. H. Pui, *Journal of Nanoparticle Research*, 2004, **6**, 313–320.

[2] H. K. Kammler, L. Mädler and S. E. Pratsinis, *Chemical Engineering & Technology*, 2001, **24**, 583–596.

[3] A. Violi and A. Venkatnathan, *The Journal of Chemical Physics*, 2006, **125**, 054302–054302–8.

[4] S. H. Chung and A. Violi, *Carbon*, 2007, **45**, 2400–2410.

[5] H. Wang, *Proceedings of the Combustion Institute*, 2011, **33**, 41–67.

[6] R. M. Laine, J. C. Marchal, H. P. Sun and X. Q. Pan, *Nature Materials*, 2006, **5**, 710–712.

[7] A. Kay and M. Grätzel, *Solar Energy Materials and Solar Cells*, 1996, **44**, 99–117.

[8] *Soots (IARC Summary & Evaluation, Volume 35)*, 1985.

[9] A. Nel, T. Xia, L. Mädler and N. Li, *Science*, 2006, **311**, 622–627.

[10] R. Chang and A. Violi, *The Journal of Physical Chemistry B*, 2006, **110**, 5073–5083.

[11] S. L. Fiedler and A. Violi, *Biophysical Journal*, 2010, **99**, 144–152.

[12] S. Choe, R. Chang, J. Jeon and A. Violi, *Biophysical Journal*, 2008, **95**, 4102–4114.

[13] P. Elvati and A. Violi, *Nanotoxicity*, Humana Press, 2012, pp. 189–202.

[14] A. E. Nel, L. Mädler, D. Velegol, T. Xia, E. M. V. Hoek, P. Somasundaran, F. Klaessig, V. Castranova and M. Thompson, *Nature Materials*, 2009, **8**, 543–557.

[15] B. Fubini, M. Ghiazza and I. Fenoglio, *Nanotoxicology*, 2010, **4**, 347–363.

[16] M. Frenklach, *Physical Chemistry Chemical Physics*, 2002, **4**, 2028–2037.

[17] J. Singh, R. I. Patterson, M. Kraft and H. Wang, *Combustion and Flame*, 2006, **145**, 117–127.

[18] A. D'Anna, *Proceedings of the Combustion Institute*, 2009, **32**, 593–613.

[19] H. Richter and J. Howard, *Progress in Energy and Combustion Science*, 2000, **26**, 565–608.

[20] C. Jäger, H. Mutschke, T. Henning and F. Huisken, *European Astronomical Society Publications Series*, 2011, **46**, 293–304.

[21] Z. A. Mansurov, *Combustion, Explosion and Shock Waves*, 2005, **41**, 727–744.

[22] Z. A. Mansurov, *Journal of Engineering Physics and Thermophysics*, 2011, **84**, 125–159.

[23] A. E. Karataş and Ö. L. Gülder, *Progress in Energy and Combustion Science*, 2012, **38**, 818–845.

[24] J. Xi and B.-J. Zhong, *Chemical Engineering & Technology*, 2006, **29**, 665–673.

[25] D. T. Gillespie, A. Hellander and L. R. Petzold, *The Journal of Chemical Physics*, 2013, **138**, 170901–170901–14.

[26] J. Appel, H. Bockhorn and M. Frenklach, *Combustion and Flame*, 2000, **121**, 122–136.

[27] G. Blanquart, P. Pepiot-Desjardins and H. Pitsch, *Combustion and Flame*, 2009, **156**, 588–607.

[28] J. A. Miller and C. F. Melius, *Combustion and Flame*, 1992, **91**, 21–39.

[29] C. Marchal, J.-L. Delfau, C. Vovelle, G. Moréac, C. Mounaïm-Rousselle and F. Mauss, *Proceedings of the Combustion Institute*, 2009, **32**, 753–759.

[30] A. Raj, I. D. C. Prada, A. A. Amer and S. H. Chung, *Combustion and Flame*, 2012, **159**, 500–515.

[31] M. Frenklach and H. Wang, *Symposium (International) on Combustion*, 1991, **23**, 1559–1566.

[32] H. Wang and M. Frenklach, *Combustion and Flame*, 1997, **110**, 173–221.

[33] Y. Wang, A. Raj and S. H. Chung, *Combustion and Flame*, 2013, **160**, 1667–1676.

[34] *CHEMKIN 10112, Reaction Design: San Diego*, 2011.

[35] A. Tregrossi, A. Ciajolo and R. Barbella, *Combustion and Flame*, 1999, **117**, 553–561.

[36] N. M. O'Boyle, M. Banck, C. A. James, C. Morley, T. Vandermeersch and G. R. Hutchison, *Journal of Cheminformatics*, 2011, **3**, 33.

[37] A. F. Voter, *Radiation Effects in Solids*, Springer Netherlands, 2007, pp. 1–23.

[38] A. Bortz, M. Kalos and J. Lebowitz, *Journal of Computational Physics*, 1975, **17**, 10–18.

[39] D. T. Gillespie, *Journal of Computational Physics*, 1976, **22**, 403–434.

[40] D. T. Gillespie, *The Journal of Physical Chemistry*, 1977, **81**, 2340–2361.

[41] *Daylight Theory: SMARTS - A Language for Describing Molecular Patterns*, 2013.

[42] M. Frenklach, D. W. Clary, W. C. Gardiner Jr. and S. E. Stein, *Symposium (International) on Combustion*, 1985, **20**, 887–901.

[43] H. Wang and M. Frenklach, *The Journal of Physical Chemistry*, 1994, **98**, 11465–11489.

[44] J. Bittner and J. Howard, *Symposium (International) on Combustion*, 1981, **18**, 1105–1116.

[45] V. V. Kislov, N. I. Islamova, A. M. Kolker, S. H. Lin and A. M. Mebel, *J. Chem. Theory Comput.*, 2005, **1**, 908–924.

[46] M. Celnik, A. Raj, R. West, R. Patterson and M. Kraft, *Combustion and Flame*, 2008, **155**, 161–180.

[47] A. Raj, M. Celnik, R. Shirley, M. Sander, R. Patterson, R. West and M. Kraft, *Combustion and Flame*, 2009, **156**, 896–913.

[48] A. Violi, *The Journal of Physical Chemistry A*, 2005, **109**, 7781–7787.

[49] A. D'Anna and A. Violi, *Symposium (International) on Combustion*, 1998, **27**, 425–433.

[50] H. Richter, S. Granata, W. H. Green and J. B. Howard, *Proceedings of the Combustion Institute*, 2005, **30**, 1397–1405.

[51] M. Sirignano, J. Kent and A. D'Anna, *Energy & Fuels*, 2013, **27**, 2303–2315.

[52] F. Pietrucci and W. Andreoni, *Physical Review Letters*, 2011, **107**, 085504.

[53] B. Zhao, Z. Yang, M. V. Johnston, H. Wang, A. S. Wexler, M. Balthasar and M. Kraft, *Combustion and Flame*, 2003, **133**, 173–188.

[54] S. E. Stein and A. Fahr, *The Journal of Physical Chemistry*, 1985, **89**, 3714–3725.

[55] M. Frenklach, C. A. Schuetz and J. Ping, *Proceedings of the Combustion Institute*, 2005, **30**, 1389–1396.

[56] G. P. Smith, D. M. Golden, M. Frenklach, N. W. Moriarty, B. Eiteneer, M. Goldenberg, C. T. Bowman, R. K. Hanson, S. Song, W. C. Gardiner Jr., V. V. i. Lissiansk and Z. Qin, *GRI-Mech 3.0*, 2000, Web Page.

[57] P. Weilmünster, A. Keller and K.-H. Homann, *Combustion and Flame*, 1999, **116**, 62–83.

Figures

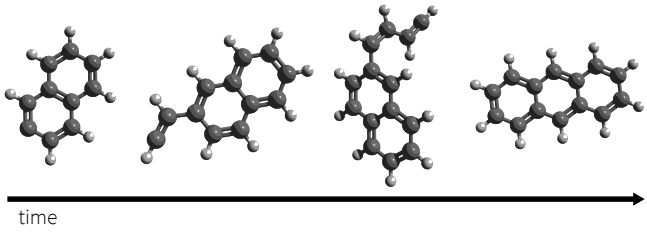

Figure 1: Selected snapshots of an example SNAPS trajectory.

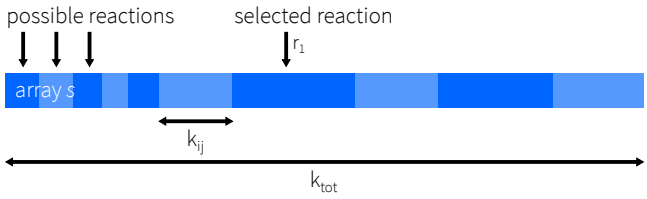

Figure 2: The BKL pathway selection algorithm.

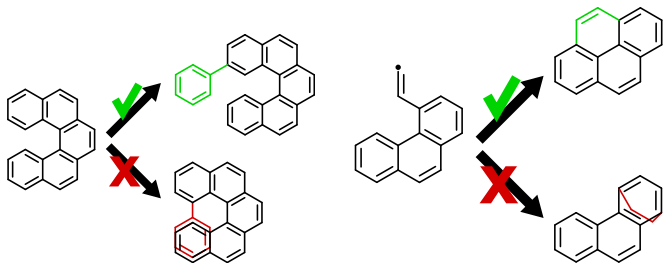

(a) (b)

Figure 3: Examples of scenarios for reaction rejection in SNAPS: (a) steric hindrance in benzene addition (b) improper ring closure.

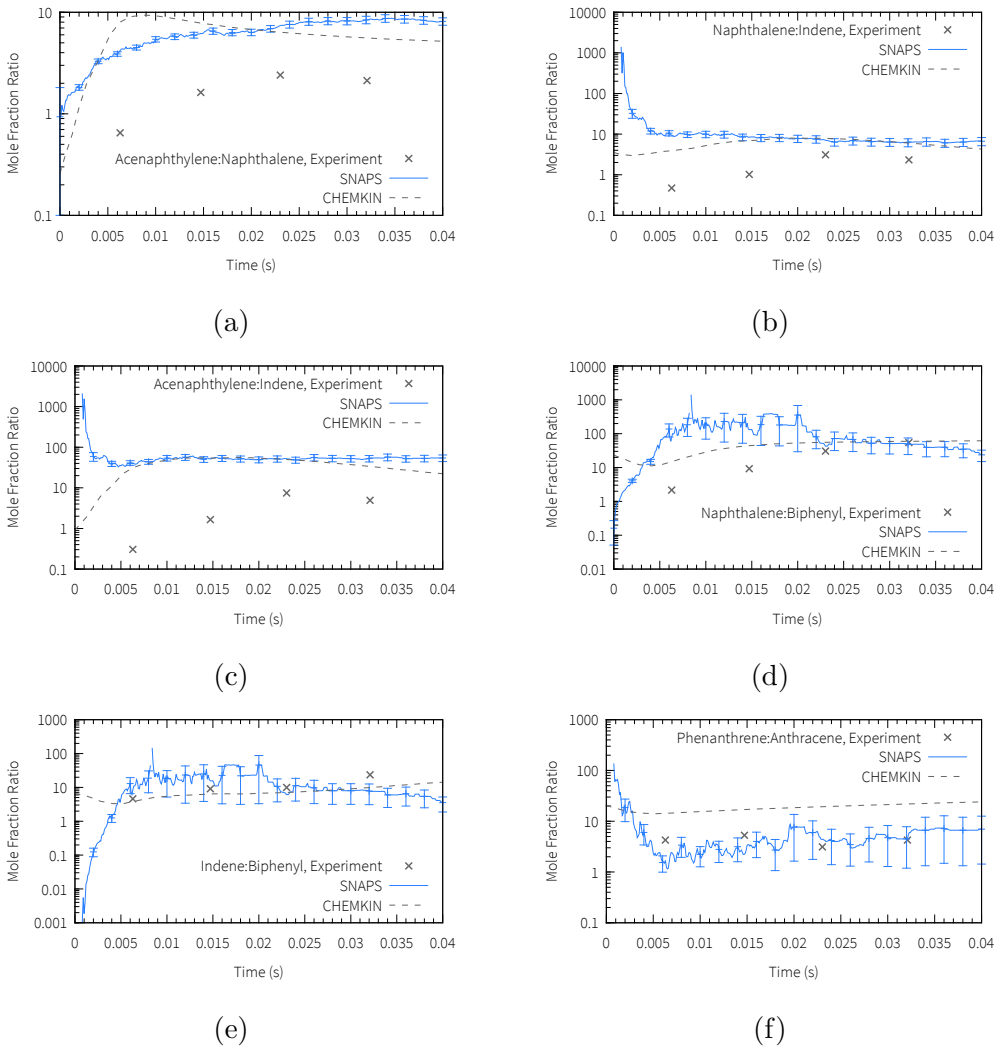

Figure 4: Time evolution of ensemble-averaged species mole fraction ratios computed with SNAPS (30000 trajectories) compared with of CHEMKIN computed and experimentally measured values in the flame of Tregrossi et al. [35]: (a) acenaphthylene:naphthalene (b) naphthalene:indene (c) acenaphthylene:indene (d) naphthalene:biphenyl (e) indene:biphenyl (f) phenanthrene:anthracene. Error bars represent the standard error of the mean.

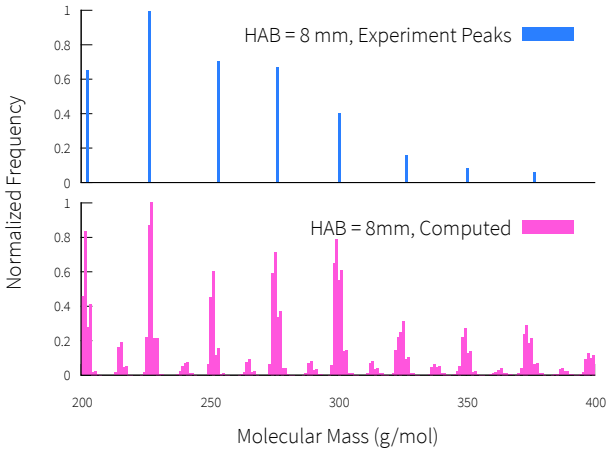

(a)

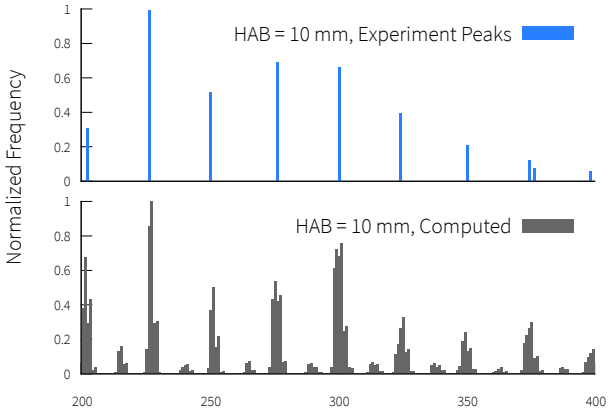

(b)

Figure 5: Comparison of ensemble-averaged mass distributions computed by SNAPS (30000 trajectories) compared with experimentally measured values in the flame of Tregrossi et al. [35]: (a) 8 mm above burner (b) 10 mm above burner.

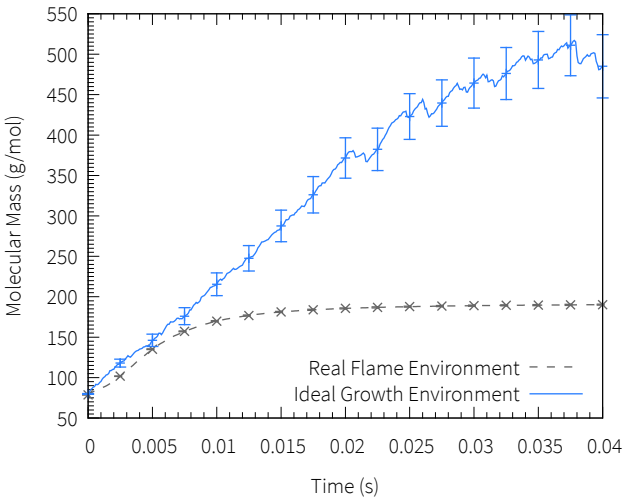

Figure 6: Comparison of average mass growth in simulations under two environments: the flame of Tregrossi et al. [35] (30000 trajectories, dashed/grey line) and ideal growth conditions (100 trajectories, continuous/blue line). Error bars represent the standard error of the mean.

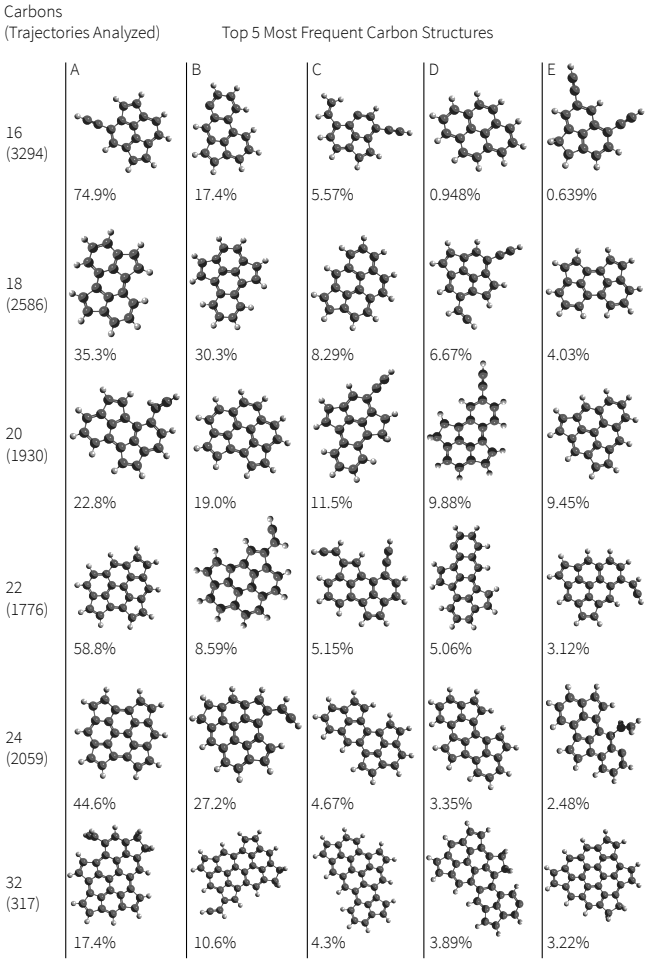

Figure 7: Top 5 most frequent carbon structures observed at 8mm above the burner (simulation time of 15 ms) in 30000 simulations for varying number of carbons. Trajectories analyzed represents the quantity of trajectories with structures matching the specified number of carbons at this height.

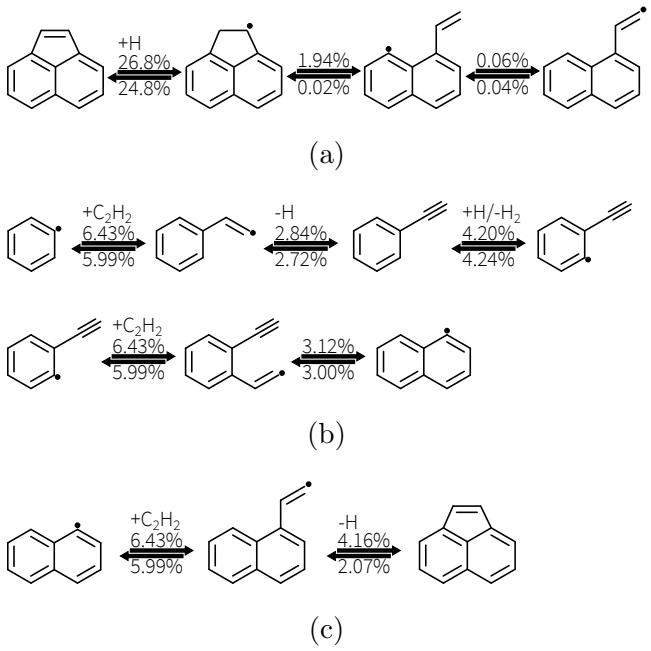

Figure 8: Important reaction pathways occuring throughout all simulations. Forward and reverse reactions are each annotated with their frequency relative to all recorded reactions. (a) 5-membered ring opening/migration pathway [55] (b) the most commonly observed 6-membered ring HACA pathway (c) acetylene addition and 5-membered ring closure at a zig zag site.